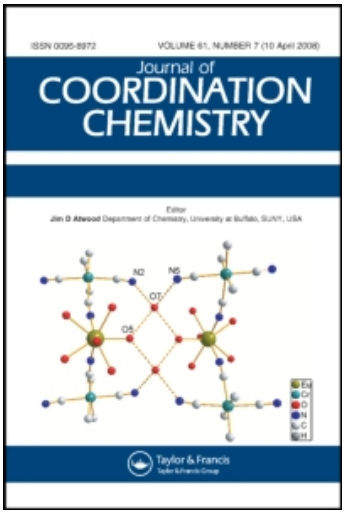

Journal of Coordination Chemistry
Publication details, including instructions for authors and subscription information:
http://www.informaworld.com/smpp/title~content=t713455674

Synthesis, characterization, cyclic voltammetry, and antimicrobial properties of *N*-(5-benzoyl-2-oxo-4-phenyl-2*H*-pyrimidine-1-yl)-malonamic acid and its metal complexes

Mehmet Sönmez[a]; Metin Çelebi[b]; Abdulkadir Levent[b]; İsmet Berber[c]; Zühre Şentürk[b]
[a] Department of Chemistry, Faculty of Science and Arts, Gaziantep University, 27310 Gaziantep, Turkey [b] Department of Chemistry, Faculty of Science and Arts, Yüzüncü Yıl University, 65080 Van, Turkey [c] Department of Biology, Faculty of Science and Arts, Sinop University, 57000 Sinop, Turkey

First published on: 14 June 2010

To cite this Article Sönmez, Mehmet , Çelebi, Metin , Levent, Abdulkadir , Berber, İsmet and Şentürk, Zühre(2010) 'Synthesis, characterization, cyclic voltammetry, and antimicrobial properties of *N*-(5-benzoyl-2-oxo-4-phenyl-2*H*-pyrimidine-1-yl)-malonamic acid and its metal complexes', Journal of Coordination Chemistry, 63: 11, 1986 — 2001, First published on: 14 June 2010 (iFirst)
To link to this Article: DOI: 10.1080/00958972.2010.494252
URL: http://dx.doi.org/10.1080/00958972.2010.494252

Journal of Coordination Chemistry
Vol. 63, No. 11, 10 June 2010, 1986–2001

Taylor & Francis
Taylor & Francis Group

Synthesis, characterization, cyclic voltammetry, and antimicrobial properties of *N*-(5-benzoyl-2-oxo-4-phenyl-2*H*-pyrimidine-1-yl)-malonamic acid and its metal complexes

MEHMET SÖNMEZ*†, METIN ÇELEBI‡, ABDULKADIR LEVENT‡, İSMET BERBER§ and ZÜHRE ŞENTÜRK‡

†Department of Chemistry, Faculty of Science and Arts, Gaziantep University, 27310 Gaziantep, Turkey
‡Department of Chemistry, Faculty of Science and Arts, Yüzüncü Yıl University, 65080 Van, Turkey
§Department of Biology, Faculty of Science and Arts, Sinop University, 57000 Sinop, Turkey

(*Received 21 December 2009; in final form 2 March 2010*)

A new heterocyclic compound, *N*-(5-benzoyl-2-oxo-4-phenyl-2*H*-pyrimidin-1-yl)-malonamic acid, was synthesized from *N*-aminopyrimidine-2-one and malonyldichloride. Bis-chelate complexes of the ligand were prepared from acetate/chloride salts of Cu(II), Co(II), Ni(II), Mn(II), Zn(II), Cd(II), Fe(III), Cr(III), and Ru(III) in methanol. The structures of the ligand and its metal complexes were characterized by microanalyses, IR, NMR, API-ES, UV-Vis spectroscopy, magnetic susceptibility, and conductometric analyses. Octahedral geometry was suggested for all the complexes, in which the metal center coordinates to ONO donors of the ligand. Each ligand binds the metal using C=O, HN, and carboxylate. The cyclic voltammograms of the ligand and the complexes were also discussed. The compounds were evaluated for their antimicrobial activities against Gram-positive and Gram-negative bacteria, and fungi using microdilution procedure. The antimicrobial studies showed that Cu(II), Fe(III), and Ru(III) complexes exhibited good antibacterial activity against Gram-positive bacteria with minimum inhibitory concentrations between 20 and 80 $\mu g\,mL^{-1}$. However, the ligand and the complexes possess weak efficacy against Gram-negative bacterium and *Candida* strains. As a result, we suggest that these complexes containing pyrimidine might be a new group of antibacterial agents against Gram-positive bacteria.

Keywords: *N*-aminopyrimidine complexes; Cyclic voltammetry; Biological activity

1. Introduction

Compounds containing pyrimidine and purine play a significant role in many biological systems [1], where both exist in nucleic acids, several vitamins, coenzymes, and antibiotics. Pyrimidine-derived metal ion complexes have been extensively investigated because of their biological activity [2–7]. Moreover, recent studies [8] showed that introduction of substituent groups at C5 and C6 positions of pyrimidine can increase

*Corresponding author. Email: vansonmez@hotmail.com

ISSN 0095-8972 print/ISSN 1029-0389 online © 2010 Taylor & Francis
DOI: 10.1080/00958972.2010.494252

the biological activity. Additionally, metal pyrimidine derivative complexes are also biologically active materials. The variety of biological applications of those compounds was correlated with the chelating property of the pyrimidine derivatives toward traces of metal ions. These provide potential binding sites for metal ions, and information on their coordination properties is important in understanding the role of the metal ions in biological systems. Many compounds of therapeutic importance contain pyrimidine ring system. Pyrimidine compounds are also used as hypnotic drugs [8, 9]. Pyrimidine nucleus is imbedded in a large number of compounds with diverse pharmacological activities, such as antitumor [10], antiviral [11], anti-inflammatory [12], antibacterial [13], and antifungal [14]. Here, we present the synthesis and properties of a new heterocyclic ligand containing pyrimidine ring and their Ni(II), Cu(II), Co(II), Mn(II), Zn(II), Cd(II), Cr(III), Fe(III), and Ru(III) complexes. All the synthesized compounds were investigated for electrochemical properties and antimicrobial activities.

2. Experimental

2.1. *Materials*

All chemicals used in this study were obtained commercially and used without purification. 1-Amino-5-benzoyl-4-phenyl-1*H*-pyrimidine-2-one (*N*-aminopyrimidine) was prepared according to a known procedure [15].

2.2. *Physical measurements*

Elemental analyses (C, H, N, and S) were performed using a Leco CHNS model 932 elemental analyzer. IR spectra were obtained using KBr discs (4000–400) cm^{-1} on a Bio-Rad-Win-IR spectrophotometer. Electronic spectra in the 200–900 nm range were obtained in DMF on a Unicam UV2-100 UV-Vis spectrophotometer. Magnetic measurements were carried out by the Gouy method using $Hg[Co(SCN)_4]$ as calibrant. Molar conductances of the Schiff-base ligand and transition metal complexes were determined in DMF at room temperature using a Jenway model 4070 conductivity meter. The ^1H- and ^{13}C-NMR spectra of the Schiff base were recorded with a Bruker 300 MHz Ultrashield TM NMR instrument. LC/MS-API-ES mass spectra were recorded using an Agilent model 1100 MSD mass spectrophotometer. Atomic absorption measurements for determination of metal ions were carried out using a Thermo Solar System Atomic Absorption Spectrophotometer. For AAS, metals were measured using the following settings: flame type air–acetylene; lamp current %75; fuel flow 0.9 l min^{-1}; burner height 12.0 mm; band pass 0.5 nm; measurement 4 s. Electrochemical measurements were carried out with a BAS 100 W electrochemical analyzer (Bioanalytical System, USA) using a three electrode cell unit, glassy carbon working electrode (Φ: 3 mm, BAS), Ag/AgCl (NaCl 3 mol L^{-1}, Model RE-1, BAS, USA) as reference electrode and platinum wire as auxiliary electrode. The reference electrode was separated from the bulk solution by a fritted-glass bridge filled with the solvent/supporting electrolyte mixture. Before each experiment, the glassy carbon electrode was polished manually with alumina (Φ: 0.01 μm). All cyclic voltammetric experiments were recorded at $25 \pm 5^{\circ}C$ in DMF and ionic strength was maintained

at 0.1 mol L^{-1} with $LiClO_4$ as the supporting electrolyte. The solutions were deoxygenated by passing dry nitrogen through the solution for 20 min prior to the experiments, and during the experiments N_2 flow was maintained over the solution.

2.3. *Synthesis of N-(benzoyl-2-oxo-4-phenyl-2H-pyrimidine-1-yl)-malonamic acid (N-PMAH)*

The ligand (*N*-PMAH) (figure 1) was prepared by condensation between *N*-aminopyrimidine and malonyldichloride. First, 1 mmol *N*-aminopyrimidine was dissolved in 40 mL hot toluene and 2 mmol triethylamine was added to this solution. Afterwards, 1 mmol (0.1 mL) malonyldichloride in 10 mL dry toluene was added slowly to this solution. A brown precipitate formed at once. This mixture was stirred at room temperature for 6 h. This precipitate was filtered off. Triethylammoniumchloride remains soluble in water. This precipitate was dissolved in sodium hydroxide solution (10%, 30 mL). After filtration, the product was obtained by precipitation with dilute hydrochloric acid. The title ligand was filtered again, washed, and dried in vacuum over P_2O_5. (*N*-(Benzoyl-2-oxo-4-phenyl-2*H*-pyrimidine-1-yl)-malonamic acid) *N*-PMAH (0.300 g, 80%), m.p. 221°C. Anal. Calcd for $C_{20}H_{15}N_3O_5$ (377): C, 63.79; H, 4.18; N, 11.28. Found (%): C, 63.66; H, 3.97; N, 11.14. Selected IR data, $\nu(cm^{-1})$: ~3360, 3250 ν(OH/NH), 1699 ν(COOH), 1680 ν(Ph–CO–), 1655 $\nu(-C{=}O)_{pyrimidine}$, 1613 $\nu(NH-C{=}O)_{amide}$; ^{1}H-NMR (DMSO-d_6), δ 12.2 (bs, 1H, COOH), 8.7 (s, H pyrimidine ring), 6.8–7.9 (m, Harm); 4.3 (sb, NH ↔ OH), 3.75 (s, $-CH_2-$) ^{13}C-NMR (DMSO-d_6), δ 191.5 (OC–Ar), 173.2 (–COOH), 154.1 (s, C=O ↔ C–OH), 165.7 (s, C4-pyrimidine ring), 152.3 (s, –C2, pyrimidine ring), 137.1 (s, –C6, pyrimidine ring), 116.4 (s, –C5, pyrimidine ring), 128.1–136.5 (m, aromatic C), 46.0 (s, aliphatic C). UV-Vis (DMF, nm): 225, 280, 312, 366. LC-MS, m/z 378 $[MH]^+$.

2.4. *Synthesis of the complexes*

2.4.1. Synthesis of $[Cu(N\text{-}PMA)_2] \cdot 2H_2O$. 0.377 g (1 mmol) of *N*-PMAH was dissolved in 30 mL of chloroform per 15 mL methanol, and a solution of 0.100 g (0.5 mmol) $Cu(CH_3COO)_2 \cdot H_2O$ in 15 mL methanol was added dropwise with continuous stirring. The mixture was stirred further for 1 h at 60°C. The light brown-green solid was filtered off, washed with diethyl ether, followed by cold methanol and

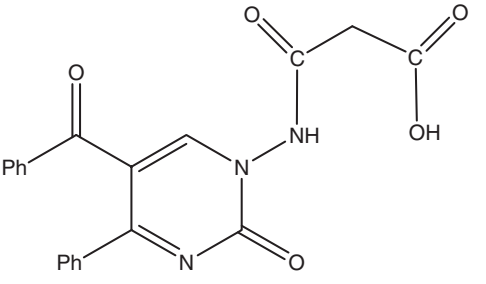

Figure 1. Structure of *N*-PMAH.

dried in a vacuum desiccator. Yield: 0.210 g (%76), m.p. 248°C. Anal. Calcd for $C_{40}H_{32}CuN_6O_{12}$ (852.26 g mol^{-1}): C, 56.32; H, 3.75; N, 9.85; Cu, 7.45. Found (%): C, 56.58; H, 4.14; N, 9.93; Cu, 8.07. Selected IR data (KBr, ν cm^{-1}): 3402 ν(NH–OH/H_2O), 1646 ν(Ph–CO) 1633, 1600 ν(C=O). μ_{eff}: 2.2 BM. Λ_M (10^{-3} mol L^{-1}, DMF, S cm^2 mol^{-1}): 8.3. UV-Vis (DMF, nm): 224, 239, 280, 297, 306, 348, 390, 591. API-ES, m/z: 851.6 [2(*N*-PMA) + ^{63}Cu + 2H_2O]$^+$; 817 [2(*N*-PMA) + ^{63}Cu]$^+$.

2.4.2. Synthesis of [Co(*N*-PMA)$_2$] · 2H$_2$O. 0.377 g (1 mmol) of *N*-PMAH was dissolved in 30 mL of chloroform per 15 mL methanol, and a solution of 0.125 g (0.5 mmol) $Co(CH_3COO)_2 \cdot 4H_2O$ in 15 mL methanol was added dropwise with continuous stirring. The mixture was stirred further for 1 h at 60°C. The precipitated pale green solid was filtered off, washed with diethyl ether, followed by cold methanol, and dried in a vacuum desiccator. Yield: 0.11 g (%26), m.p. 291°C. Anal. Calcd for $C_{40}H_{32}CoN_6O_{12}$ (847.14 g mol^{-1}): 56.68; H, 3.81; N, 9.91; Co, 6.95. Found (%): C, 56.52; H, 3.96; N, 9.40; Co, 6.42. Selected IR data (KBr, ν cm^{-1}): 3402 ν(NH–OH/H_2O), 1666 ν(Ph–CO), 1614 ν(C=O). μ_{eff}: 4.77 BM. Λ_M (10^{-3} M, DMF, S cm^2 mol^{-1}): 18.5. UV-Vis (DMF, nm): 223, 268, 308, 338, 393, 407, 686, 789. API-ES, m/z: 846.3 [2(*N*-PMA) + ^{59}Co + 2H_2O]$^+$; 810 [2(*N*-PMA) + ^{59}Co]$^+$.

2.4.3. Synthesis of [Ni(*N*-PMA)$_2$] · 4H$_2$O. 0.377 g (1 mmol) of *N*-PMAH was dissolved in 30 mL of chloroform per 15 mL methanol, and a solution of 0.125 g (0.5 mmol) $Ni(CH_3COO)_2 \cdot 4H_2O$ in 15 mL methanol was added dropwise with continuous stirring. The mixture was stirred further for 1 h at 60°C. The precipitated brown solid was filtered off, washed with diethyl ether, followed by cold methanol, and dried in a vacuum desiccator. Yield: 0.200 g (%46), m.p. 277°C. Anal. Calcd for $C_{40}H_{36}N_6NiO_{14}$ (882.16 g mol^{-1}): C, 54.38; H, 4.11; N, 9.51; Ni, 6.64. Found (%): C, 54.04; H, 4.26; N, 10.10; Ni, 6.97. Selected IR data (KBr, ν cm^{-1}): 3400–3216 (OH/H_2O–NH), ~1650, 1600 (C=O). μ_{eff}: 3.36 BM. Λ_M (10^{-3} M, DMF, S cm^2 mol^{-1}): 12.5. UV-Vis (DMF, nm): 241, 286, 309, 322, 386, 407, 560. API-ES, m/z: 811 [2(*N*-PMA) + ^{60}Ni]$^+$.

2.4.4. Synthesis of [Mn(*N*-PMA)$_2$] · 3H$_2$O. 0.377 g (1 mmol) of *N*-PMAH was dissolved in 30 mL of chloroform per 15 mL methanol, and a solution of 0.114 g (0.5 mmol) $Mn(CH_3COO)_2 \cdot 3H_2O$ in 15 mL methanol was added dropwise with continuous stirring. The mixture was stirred further for 1 h at 60°C. The precipitated light brown solid was filtered off, washed with diethyl ether, followed by cold methanol, and dried in a vacuum desiccator. Yield: 0.110 g (%26), m.p. 291°C. Anal. Calcd for $C_{40}H_{34}MnN_6O_{13}$ (861.16 g mol^{-1}): C, 55.76; H, 3.98; N, 9.75; Mn, 6.38. Found (%): C, 55.60; H, 4.12; N, 9.55; Mn, 5.95. Selected IR data (KBr, ν cm^{-1}): 3414 (OH/H_2O–NH), 3260 (NH), 1653, 1640, 1617 (C=O). μ_{eff}: 5.68 BM. Λ_M (10^{-3} mol L^{-1}, DMF, S cm^2 mol^{-1}): 9.5. UV-Vis (DMF, nm): 215, 273, 315, 352, 395, and 402. API-ES, m/z: 807[2(*N*-PMA) + ^{55}Mn]$^+$.

2.4.5. Synthesis of [Cd(*N*-PMA)$_2$] · 3H$_2$O. 0.377 g (1 mmol) of *N*-PMAH was dissolved in 30 mL of chloroform per 15 mL methanol, and a solution of 0.125 g (0.5 mmol) $CdCl_2 \cdot 2H_2O$, and 2 mmol CH_3COONa 15 mL methanol was added

dropwise with continuous stirring. The mixture was stirred further for 1 h at 60°C. The precipitated orange solid was filtered off, washed with diethyl ether, followed by cold methanol, and dried in a vacuum desiccator. Yield: 0.120 g (%26), m.p. 291°C. Anal. Calcd for $C_{40}H_{32}CdN_6O_{13}$ (920.12 g mol^{-1}): C, 52.15; H, 3.69; N, 9.12; Cd, 12.21. Found (%): C, 52.27; H, 3.73; N, 9.14; Cd, 11.94. Selected IR data (KBr, ν cm^{-1}): 3400 (OH/H_2O–NH), 3264 (NH), 1658, 1633, 1599 (C=O). ^{1}H-NMR (DMSO), δ 9.0 (s, NH), 8.8 (s, C–H pyrimidine), 6.7–7.9 (m, Harm), 3.5 (m, H_2O), 3.2 (s, –CH_2–); ^{13}C-NMR (DMSO), δ 193.1, 174.5, 160.1, 153.0, 151.9, 127.1–138.4, 114.1, 43.2. μ_{eff}: Dia. Λ_M (10^{-3} mol L^{-1}, DMF, S cm^2 mol^{-1}): 9.5. UV-Vis (DMF, nm): 225, 278, 318, 338, 380. API-ES, *m*/*z*: 918 [2(*N*-PMA) + ^{112}Cd + 3H_2O]$^+$.

2.4.6. Synthesis of [Zn(*N*-PMA)$_2$] · 4H$_2$O. 0.377 g (1 mmol) of *N*-PMAH was dissolved in 30 mL of chloroform per 15 mL methanol, and a solution of 0.110 g (0.5 mmol) $Zn(CH_3COO)_2 \cdot 2H_2O$ in 15 mL methanol was added dropwise with continuous stirring. The mixture was stirred further for 1 h at 60°C. The precipitated pale yellow solid was filtered off, washed with diethyl ether, followed by cold methanol, and dried in a vacuum desiccator. Yield: 0.110 g (%25), m.p. 286°C. Anal. Calcd for $C_{40}H_{36}N_6O_{14}Zn$ (888.16 g mol^{-1}): C, 53.97; H, 4.08; N, 9.44; Zn, 7.35. Found (%): C, 53.53; H, 3.80; N, 9.70; Zn, 8.02. Selected IR data (KBr, ν cm^{-1}): ~3350 (OH/H_2O–NH), 1651, 1600 (C=O). ^{1}H-NMR (DMSO), δ 9.2 (s, NH), 8.8 (s, C–H pyrimidine), 6.7–8.0 (m, Harm), 3.5 (m, H_2O), 3.3 (s, –CH_2–); ^{13}C-NMR (DMSO), δ 191.0, 174.7, 165.3, 161.3, 150.8, 126.9–137.4, 115.0, 43.8. μ_{eff}: Dia. Λ_M (10^{-3} mol L^{-1}, DMF, S cm^2 mol^{-1}): 5.2. UV-Vis (DMF, nm): 223, 246, 277, 325, 368, 389. API-ES, *m*/*z*: 816 [2(*N*-MPA) + ^{64}Zn]$^+$.

2.4.7. Synthesis of [Fe(*N*-PMA)$_2$]Cl · 2H$_2$O. 0.377 g (1 mmol) of *N*-PMAH was dissolved in 30 mL of chloroform per 15 mL methanol, and a solution of 0.082 g (0.5 mmol) $FeCl_3$ in 15 mL methanol was added dropwise with continuous stirring. The mixture was stirred further for 1 h at 60°C. The precipitated light brown solid was filtered off, washed with diethyl ether, followed by cold methanol, and dried in a vacuum desiccator. Yield: 0.165 g (%38), m.p. 253°C. Anal. Calcd for $C_{40}H_{32}ClFeN_6O_{12}$ (881.29 g mol^{-1}): C, 54.46; H, 3.63; N, 9.53; Fe, 6.34. Found (%): C, C, 54.80; H, 3.85; N, 9.44; Fe, 7.01. Selected IR data (KBr, ν cm^{-1}): 3400 (OH/H_2O), 3270 (NH), 1661, 1630, 1600 (C=O). μ_{eff}: 5.74 BM. Λ_M (10^{-3} mol L^{-1}, DMF, S cm^2 mol^{-1}): 58.2. UV-Vis (DMF, nm): 240, 288, 308, 346, 381, 419, 538. API-ES, *m*/*z*: 808 [2(*N*-PMA) + ^{56}Fe]$^+$.

2.4.8. Synthesis of [Cr(*N*-PMA)$_2$]Cl · H$_2$O. 0.377 g (1 mmol) of *N*-PMAH was dissolved in 30 mL of chloroform per 15 mL methanol, and a solution of 0.080 g (0.5 mmol) $CrCl_3$ in 15 mL methanol was added dropwise with continuous stirring. The mixture was stirred further for 1 h at 60°C. The precipitated light brown solid was filtered off, washed with diethyl ether, followed by cold methanol, and dried in a vacuum desiccator. Yield: 0.108 g (%25), m.p. 232°C. Anal. Calcd for $C_{40}H_{30}ClCrN_6O_{11}$ (859.45 g mol^{-1}): C, 55.85; H, 3.50; N, 9.77; Cr, 6.05. Found (%): C, 56.30; H, 4.00; N, 10.00; Cr, 5.78. Selected IR data (KBr, ν cm^{-1}): 3414 (OH/

H_2O–NH), 1656, 1620 (C=O). μ_{eff}: 3.82 BM. Λ_M (10^{-3} mol L^{-1}, DMF, S cm^2 mol^{-1}): 50.1. UV-Vis (DMF, nm): 248, 262, 335, 436, 601.

2.4.9. Synthesis of [Ru(*N*-PMA)$_2$]Cl · 3H$_2$O. 0.377 g (1 mmol) of *N*-PMAH was dissolved in 30 mL of chloroform per 15 mL methanol, and a solution of 0.104 g (0.5 mmol) $RuCl_3$ in 15 mL methanol and water was added dropwise with continuous stirring. The mixture was stirred further for 1 h at 60°C. The precipitated light dark green solid was filtered off, washed with diethyl ether, followed by cold methanol, and dried in a vacuum desiccator. Yield: 0.130 g (%28), m.p. 234°C. Anal. Calcd for $C_{40}H_{34}ClRuN_6O_{13}$ (943.1 g mol^{-1}): C, 50.93; H, 3.63; N, 8.91. Found (%): C, 50.86; H, 3.72; N, 8.96. Selected IR data (KBr, ν cm^{-1}): 3400 (OH/H_2O), ~3250 (NH), 1660, 1630, 1600 (C=O). μ_{eff}: 1.67 BM. Λ_M (10^{-3} mol L^{-1}, DMF, S cm^2 mol^{-1}): 74.0. UV-Vis (DMF, nm): 225, 271, 307, 356, 375, 395, 539, 666. API-ES, *m*/*z*: 927 $[2(N\text{-PMA}) + {}^{101}Ru + {}^{35}Cl + 2H_2O]^+$, 888.2 $[2(N\text{-PMA}) + {}^{101}Ru + {}^{35}Cl]^+$; 952.7 $[2(N\text{-PMA}) + {}^{101}Ru]^+$.

2.5. *Biological assay*

2.5.1. Compounds and cells. Test compounds were dissolved in DMSO (12.5%) at an initial concentration of 1280 μg mL^{-1} and then they were serially diluted in culture medium. Bacterial strains were supplied from American Types Culture Collection. *Candida* strains were obtained from Refik Saydam Hifsisihha Research Institute, Ankara, Turkey. These microorganisms were stored in 10% sterile glycerol suspensions at −70°C.

2.6. *Antibacterial assay*

Newly synthesized ligand and its metal complexes were screened for their *in vitro* antibacterial activity against four Gram-positive (*Staphylococcus aureus* ATCC 6538, *S. aureus* ATCC 25923, *Bacillus cereus* ATCC 7064, and *Micrococcus luteus* ATCC 9345) and one Gram-negative (*Escherichia coli* ATCC 4230) bacteria by using the microdilution broth procedure [16]. Ampicillin trihydrate was used as reference antibacterial drug. Stock solutions of the compounds and reference drug were dissolved in 12.5% DMSO, which had no effect on the microorganisms in the studied concentration. Further dilutions of the compounds and standard antibacterial agent were prepared with Mueller-Hinton broth (Difco) medium, at pH 7.2 as outlined in NCCLS approved standard document M7-A4 [16]. The final concentrations of all the compounds and the reference drug ranged from 1280, 640, 320, 160, 80, 40, 20, 10, 5 > μg mL^{-1}. DMSO was used as negative control. Prior to minimum inhibitory concentration (MIC) assay, each microorganism was grown at least twice on Mueller-Hinton agar (Difco) to ensure optimal growth characteristics. Then, the bacterial inoculums were adjusted to 0.5–2.5 × 10^3 cells mL^{-1} by spectrophotometric method in Mueller–Hinton broth medium, and an aliquot of 100 μL was added to each tube of the serial dilution [17, 18]. The chemical compounds-broth medium serial tube dilutions inoculated with each bacterium were incubated on a rotary shaker at 37°C for 24 and 48 h at 150 rpm. The MIC endpoints were read visually, and the values of each

chemical compounds were determined as the lowest concentration of each chemical compounds in the tubes with no growth (i.e. no turbidity) of inoculated bacteria.

2.7. *Antifungal assay*

The antifungal activities were tested against three yeast (*Candida albicans* ATCC 14053, *C. krusei* ATCC 6258, and *C. parapsilosis* ATCC 22019) strains by using the microdilution broth procedure [19]. Fluconazole was used as reference antifungal drug. Stock solutions of the compounds and reference drug were dissolved in 12.5% DMSO, which had no effect on the microorganisms in the studied concentration. Further dilutions of the compounds and standard antifungal drug were prepared with RPMI 1640 medium (Sigma) which was buffered to pH 7.0 with 0.165 mol L^{-1} morpholinopropanesulfonic acid (Sigma) according to the guidelines in NCCLS approved standard document M27-A2 [19]. The final concentrations of all the compounds and the reference drug ranged from 1280, 640, 320, 160, 80, 40, 20, 10, 5 μg mL^{-1}. DMSO was used as negative control. Prior to MIC assay, each microorganism was grown at least twice on Sabouraud dextrose agar (Difco) to ensure optimal growth characteristics. Then, the yeast inoculums were adjusted to concentration of 0.5–2.5 × 10^3 cells mL^{-1} by spectrophotometric method in RPMI 1640 medium, and an aliquot of 100 μL was added to each tube of the serial dilution [17–19]. The compounds-broth medium serial tube dilutions inoculated with yeast were incubated on a rotary shaker at 35°C for 24 and 48 h at 150 rpm. The MIC endpoints were read visually, and the values of each compound were determined as the lowest concentration in the tubes with no growth (i.e. no turbidity) of inoculated fungi.

2.8. *Statistical analysis*

Bioactivity data were expressed as means ±SD of means ($\bar{X} \pm SE$) of triplicates by using SPSS software version 9.0 for Windows.

3. Results and discussion

3.1. *Synthesis*

A new tridentate monoanionic ligand *N*-PMAH having ONO donors was synthesized by 1 : 1 condensation of *N*-aminopyrimidine with malonyldichloride in dry toluene. The ligand is soluble in DMSO, DMF, CH_3CN, CH_2Cl_2 and partly soluble in $CHCl_3$, MeOH, EtOH, H_2O, but insoluble in *n*-hexane and diethyl ether. The complexation of *N*-PMAH towards M(II) and M(III) were investigated. All complexes with deprotonated forms of *N*-PMAH, $[Cu(N\text{-}PMA)_2]\cdot 2H_2O$, $[Co(N\text{-}PMA)_2]\cdot 2H_2O$, $[Ni(N\text{-}PMA)_2]\cdot 4H_2O$, $[Mn(N\text{-}PMA)_2]\cdot 3H_2O$, $[Zn(N\text{-}PMA)_2]\cdot 4H_2O$, $[Cd(N\text{-}PMA)_2]\cdot 3H_2O$, $[Fe(N\text{-}PMA)_2]Cl\cdot 2H_2O$, $[Cr(N\text{-}PMA)_2]Cl\cdot H_2O$ and $[Ru(N\text{-}PMA)_2]Cl\cdot 3H_2O$ were obtained from a refluxing mixture of the respective ligand and appropriate metal salts in a 1 : 2 molar ratio in methanol. The complexes presented in figures 2 and 3 were formed in a condensation reaction of equimolar amounts of a malonyldichloride with

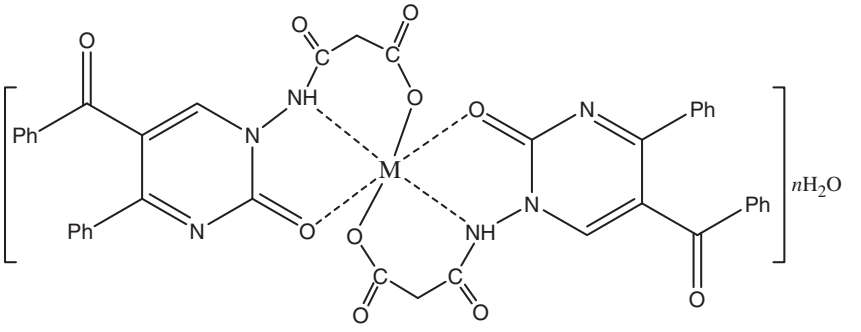

M=Cu(II), Co(II), Ni(II), Mn(II), Zn(II) and Cd(II)

Figure 2. Suggested structure of the M(II) complexes.

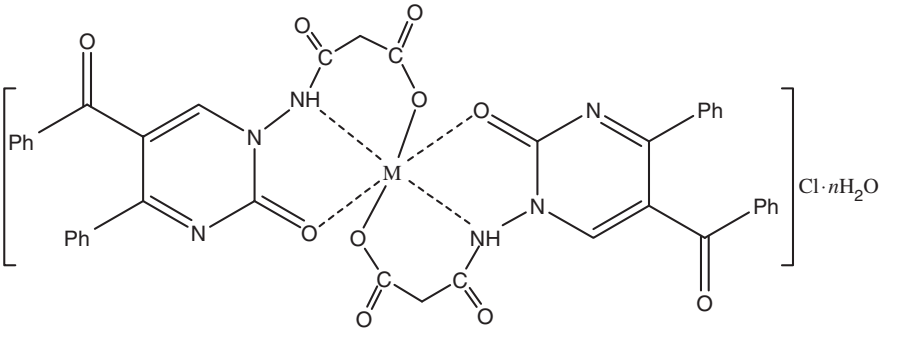

M=Cr(III), Fe(III) and Ru(III)

Figure 3. Suggested structure of the M(III) complexes.

N-aminopyrimidine and pyridine/triethylamine in dry toluene. The complexes are soluble in DMF and DMSO but sparingly soluble in common organic solvents. The melting points, yields, colors, magnetic susceptibility, molar conductivity values, and elemental analyses of complexes, and ligand are given in the section 2. The molar conductances of the complexes in DMF (10^{-3} mol L^{-1}) were in the range 5.2–18.5 Ω^{-1} cm^2 mol^{-1}, indicating their non-electrolytic nature, with the exception of the Fe(III), Cr(III), and Ru(III) complexes, which are 1 : 1 electrolytes.

3.2. *Characterization of the N-PMAH and metal complexes*

3.2.1. Infrared spectral study. Derivatives of carboxylic acids are characterized by several intense absorptions in the infrared spectrum [20]. The most prominent are in the carbonyl stretching region (1700–1725 cm^{-1}). Their exact position depends on the type of acid derivative. In addition to the carbonyl stretching absorption, the acids themselves exhibit a strong, broad O-H stretch over the range 3500–2500 cm^{-1}. Bands at 3360 and 1699 cm^{-1} are characteristic of the OH and carboxyl groups present

in the free ligand [21]. The disappearance of the 1699 cm^{-1} band suggests coordination of carboxylic oxygen after deprotonation [22]. The spectrum of the ligand shows a broad band at 3250 cm^{-1} due to asymmetric and symmetric –NH stretching frequency of the –NH group [23]. A comparison of IR spectra of the complexes with that of free ligand shows 15–60 cm^{-1} in these modes, respectively, indicating coordination through the amide nitrogen [23]. The spectrum of the ligand shows a strong band at 1680 cm^{-1} for ν(Ph–CO–), stretching vibration [2, 24].

Strong bands at 1655 and 1613 cm^{-1} in IR spectra of the free ligand assigned to $\nu(C{=}O)_{pyrimidine}$ and $\nu(NH{-}C{=}O)_{amide}$ [2, 4, 22] are changed by $\pm$10–30 cm^{-1} in spectra of complexes, indicating coordination through carbonyl oxygen and amidic nitrogen of *N*-PMAH (figure 1). In spectra of all the complexes, bands in the 445–470 and 420–426 cm^{-1} region may be due to ν(M–N) and ν(M–O), respectively [19–24]. Water content was also identified by elemental and thermal gravimetric analyses. Broad bands of all the complexes at 3240–3350 cm^{-1} are assigned to ν(OH) of water [4, 19–24].

3.2.2. UV-Vis spectral study. Electronic spectra of complexes were recorded in DMF. The Zn(II) and Cd(II) complexes, which are diamagnetic, had bands in the 280–250 nm range due to $n \rightarrow \pi^*$ and $\pi \rightarrow \pi^*$ transitions of the benzene, pyrimidine rings, and carbonyl group, respectively. In spectra of the complexes, less intense and broad bands in the 445–250 nm range result from overlap of the low-energy $\pi \rightarrow \pi^*$ transitions mainly localized within the amine chromophore and the LMCT (ligand to metal charge transfer bands) from the electronic lone pairs of the carboxylate oxygen to the M^{2+} ions [25].

Spectra of $[Cu(N\text{-PMA})_2]\cdot 2H_2O$ exhibit three broad bands at 348, 390, and 591 nm. The lower energy band may be assigned to the $^2E_g \rightarrow {}^2T_{2g}$ transition for distorted octahedral configuration [26]. The bands in the region 390 and 348 nm can be attributed to ligand $\rightarrow$ metal charge transfer. The observed magnetic moment of the Cu(II) complex (2.2 BM) indicates monomer, which is further supported by the microanalytical and API-ES mass spectral data. The higher value of μ_{eff} may be due to an intermolecular cooperative effect [27].

The spectrum of the $Ni(N\text{-PMA})_2]\cdot 4H_2O$ complex is characteristic of octahedral geometry and bands at 560 and 407 nm can be assigned to $^3A_{2g} \rightarrow {}^3T_{1g}$ (F) and $^3A_{2g} \rightarrow {}^3T_{2g}$(F) transitions. The room temperature $\mu_{eff} = 3.1$ BM and the spectral data support O_h geometry [26]. Magnetic behavior of octahedral nickel(II) complex is relatively simple. Ni(II) has the electronic configuration $3d^8$ and should exhibit a magnetic moment higher than expected for two unpaired electrons in octahedral (2.8–3.2 BM).

The electronic spectrum of $[Co(N\text{-PMA})_2]\cdot 2H_2O$ shows several intense bands between 223 and 308 nm assigned to intra-ligand transitions in ligands, while weak bands at 407, 686, and 789 nm are assigned to d–d transitions for the octahedral cobalt(II). Octahedral cobalt(II) complexes, however maintain a large contribution due to $^4T_{2g}$ ground term and exhibit μ_{eff} in the range 4.8–5.6 BM [28]. The magnetic measurement on the complex reported here, 4.77 BM, shows three unpaired electrons in a high-spin octahedral configuration. The bands observed at 338 and 393 nm are assigned to Co $\rightarrow$ L charge transfer [28].

The electronic spectrum of the Mn(II) complex of *N*-PMAH has bands in the region 395–402 nm due to $^6A_{1g} \rightarrow {}^4T_{1g}$ (4G) (ν_1), $^6A_{1g} \rightarrow {}^4$Eg (4G) ($\nu_2$), $^6A_{1g} \rightarrow {}^4T_{2g}$ (4D) (ν_3),

$^6A_{1g} \rightarrow {}^4T_{1g}$ (4P) (ν_4) transitions, respectively, indicating octahedral geometry [20], for this complex. The magnetic moment for Mn(II) complex is 5.68 BM, which is well within the range expected for octahedral geometry around the central metal ion [29].

[Fe(*N*-PMA)$_2$]Cl · 2H$_2$O has three bands at 381, 419, and 538 nm. The first band is due to $n \rightarrow \pi^*/\pi \rightarrow \pi^*$ electronic transition of the free ligand. The bands at 419 and 538 nm and its effective room temperature magnetic moment $\mu_{eff} = 5.74$ BM are assigned to octahedral structure [26].

The electronic spectrum in DMF of [Cr(*N*-PMA)$_2$]Cl · H$_2$O is expected to show three spin-allowed d–d transitions, namely $^4A_{2g}(F) \rightarrow {}^4T_{2g}$ (ν_1), $^4A_{2g} \rightarrow {}^4T_{1g}(F)$ (ν_2) and $^4A_{2g} \rightarrow {}^4T_{1g}(P)$ (ν_3). Three bands at 601 (ν_1), 436 (ν_2), and 335 (ν_3) nm suggest octahedral geometry around Cr(III) with $^4A_{2g}$ ground state [26]. The magnetic moment value (3.82 BM) for the Cr(III) complex is in agreement with the values reported for octahedral geometry around Cr(III) [30].

Low-spin Ru(III) is a d^5 system with a ground state $^2T_{2g}$ and the first excited doublet levels, in order of increasing energy, are $^2A_{2g}$ and $^2A_{1g}$, arising from a $t_{2g}^4\ e_g^1$ configuration [30, 31]. In most UV-spectra of [Ru(*N*-PMA)$_2$]Cl · 3H$_2$O complexes, only charge transfer bands are visible [26], characteristic of octahedral geometry [32, 33]. The spectra of the Ru(III) complex displayed bands at 666 and 539 nm, assigned to $^2T_{2g} \rightarrow {}^4T_{1g}$ and $^2T_{2g} \rightarrow {}^4T_{2g}$. The two lowest energy absorptions corresponding to $^2T_{2g} \rightarrow {}^4T_{1g}$ and $^2T_{2g} \rightarrow {}^4T_{2g}$ were frequently observed as shoulders on the charge transfer bands. The magnetic moments for all complexes of Ru(III) are 1.67 BM [34], corresponding to one unpaired electron.

3.2.3. ^{1}H- and ^{13}C-NMR spectral study. To identify the structure of *N*-PMAH, the ^{1}H and ^{13}C-NMR spectra were recorded in DMSO-d$_6$. The chemical shifts are given in the section 2. In ^{1}H-NMR spectra, multiplets at 6.80–7.90 ppm could be attributed to phenyl protons. The chemical shift at 12.26 ppm was assigned to the proton of carboxyl (COOH) as a singlet. Resonances with the expected integrated intensities were observed as a singlet at 4.32 (1H) and 8.70 (1H) ppm for the NH $\leftrightarrow$ OH and pyrimidine ring's proton, respectively. The –CH$_2$– protons of the ligand were observed at 3.70 ppm. The ^{1}H-NMR spectral data of the ligand were supported by the ^{13}C-NMR spectrum. The chemical shifts for the carbons of the aromatic rings were recorded between 128.15 and 136.54 ppm. The signal for the carbon of –COOH was observed at 173.23 ppm, also confirming the structure of the ligand. Signals at 191.5, 165.7, 154.1, 152.3, and 137.1 ppm were attributed to OC–Ar, (C=O $\leftrightarrow$ C–OH), C(4)pirimidine ring, C(2)pyrimidine ring, and C(6)pyrimidine ring, respectively. The chemical shift which belongs to the –CH$_2$– group was at 46.0 ppm. All protons and carbons were in their expected regions and are in agreement with values previously reported [2, 20, 24].

The Zn(II) and Cd(II) complexes (figure 2) by ^{1}H-NMR in DMSO-d$_6$ are in agreement with the proposed coordination through the carboxylic group (disappearance of the H–OOC– signal in ^{1}H-NMR spectrum) and the peaks characteristic for water molecules were observed around δ 3.52 ppm.

3.2.4. API-ES mass spectral studies. The API-ES mass spectrum of *N*-PMAH showed a molecular ion peak *m*/*z* at 378 which is equivalent to its molecular weight. The fragmentation peaks at *m*/*z* 351, 292 and 277 are ascribed to the cleavage of CO, $C_2H_2O_2$, and NH_2, respectively. The spectrum of [Cu($C_{20}H_{14}N_3O_5$)$_2$] · 2H$_2$O,

$[Ni(C_{20}H_{14}N_3O_5)_2]\cdot 4H_2O$, $[Co(C_{20}H_{14}N_3O_5)_2]\cdot 2H_2O$, $[Mn(C_{20}H_{14}N_3O_5)_2]\cdot 3H_2O$, $[Cd(C_{20}H_{14}N_3O_5)_2]\cdot 3H_2O$, and $[Ru(C_{20}H_{14}N_3O_5)_2]Cl\cdot 2H_2O$ showed a hydrated molecular ion peak at m/z 851, 884, 846, 860, 918, and 927, respectively, that is equivalent to its molecular weight. The Cu(II), Ni(II), Co(II), Mn(II), Zn(II), Cd(II), and Ru(III) complexes gave a fragment ion peak with loss of 2, 4, 2, 3, 4, 3, and 2 hydrates molecules at m/z 817, 814, 810, 806, 816, 864, 808, and 888, respectively. In case of Fe(III) and Ru(III) complexes, the peaks observed at m/z 808 and 853 were due to loss of one chlorine atom and water. The spectra of Cu(II) complex contained a number of fragments containing copper in the 3 : 1 natural abundance of ^{63}Cu and ^{65}Cu isotopes. All these fragments leading to formation of the species $[M(N\text{-PMA})_2]^+$ which undergoes demetallation to form the species $[N\text{-PMA}]^+$ gave fragment ion peak at m/z 377.

3.2.5. Electrochemical studies. The electrochemical properties of *N*-PMAH and its metal complexes at 9×10^{-4} mol L^{-1} were investigated at a glassy carbon electrode in DMF containing 0.1 mol L^{-1} $LiClO_4$, by cyclic voltammetry (CV). The electrochemical data with peak potentials are reported in table 1.

In the potential range of −2.3 V to +1.2 V at 100 mV s^{-1}, the CV of *N*-PMAH was characterized by four cathodic waves (Ic, IIc, IIIc, and IVc) with their anodic partners (Ia, IIa, IIIa, and IVa) (figure 4a). After the first voltammetric cycle, the current intensities of the reduction peaks (especially peak IIIc) decreased while the intensities of the anodic waves Ia and IIa increased slightly. The cathodic wave IIIc (−1.79 V) was also in the form of a peak and was easily measurable. Hence, all the subsequent studies were based on the measurement of the magnitude of this step. A plot of logarithm of peak current *versus* logarithm of scan rate gave a straight line (correlation coefficient 0.999) with a slope of 0.497, very close to the theoretical value of 0.5, which is expected for an ideal solution species [35]; in this case the process had a diffusive component. Taking into account the reported data concerning electrochemical behavior of recently synthesized pyrimidine compounds, such as 1-amino-5-benzoyl-4 phenyl-1H-pyrimidine-2-one [36] and *N*-(5-benzoyl-2-oxo-4-phenyl-2*H*-pyrimidin-1-yl)-oxalamic acid [2] at hanging mercury drop and glassy carbon electrodes, respectively, we might assume that the reduction steps of ligand were located on the secondary amino and the carbonyl group of the pyrimidine ring at positions 1 and 2, respectively.

Table 1. Voltammetric results in V *vs.* Ag/AgCl. Scan rate, 100 mV s^{-1}. *E*c: cathodic, *E*a: anodic.

Compound	*E*c	*E*a
N-PMAH	**Ic**, −1.32; **IIc**, −1.50; **IIIc**, −1.79; **IVc**, −1.96	**Ia**, −1.66; **IIa**, −1.21; **IIIa**, +0.22; **IVa**, +0.93
$[Cu(N\text{-PMA})_2]\cdot 2H_2O$	**I′c**, −0.48; **II′c**, −1.52; **III′c**, −2.16	**I′a**, −0.53; **II′a**, +0.86; **III′a**, −1.12
$[Co(N\text{-PMA})_2]\cdot 2H_2O$	**Ic + Iic**, −1.42; **IIIc**, −1.80	**Ia**,−1.67; **Iia**, −1.35; **Iva**, +0.79
$[Mn(N\text{-PMA})_2]\cdot 3H_2O$	**Ic + Iic**, −1.42; **IIIc**, −1.83; **Ivc**, −1.95	**Ia**, −1.61; **Iia,** −1.33
$[Ni(N\text{-PMA})_2]\cdot 4H_2O$	**Ic**, −1.25; **Iic**, −1.56; **IIIc**, −1.81; **Ivc**, −1.96	**Ia**, −1.67; **Iia,** −1.35
$[Zn(N\text{-PMA})_2]\cdot 4H_2O$	**Ic + Iic**, −1.41; **IIIc**, −1.82	**Ia**, −1.68; **Iia,** −1.29
$[Cd(N\text{-PMA})_2]\cdot 3H_2O$	**Ic + Iic**, −1.42; **IIIc**, −1.83; **Ivc**, −1.95	**Ia**, −1.62; **Iia,** −1.43
$[Fe(N\text{-PMA})_2]Cl\cdot 2H_2O$	**Ic + IIc**, −1.36; **IIIc**, −1.80; **IVc**, −1.99	**Ia**, −1.65; **IIa**, −1.28; **Iva**, +1.01
$[Cr(N\text{-PMA})_2]Cl\cdot H_2O$	**Ic**, −1.25; **Iic**, −1.55; **IIIc**, −1.80; **Ivc**, −1.99	**Ia**, −1.65; **Iia**, −1.25
$[Ru(N\text{-PMA})_2]Cl\cdot 3H_2O$	**Ic**, −1.30; **IIc**, −1.55; **IIIc**, −1.81; **IVc**, −2.00	**Ia**, −1.64; **Iia,** −1.26

The voltammograms of metal complexes investigated in the same experimental conditions, except for copper(II) complex, closely matched the voltammogram of the ligand. For this reason the waves seen in the CVs (data not shown) were presumed to be ligand based oxidation. For the cobalt(II), manganese(II), zinc(II), cadmium(II) and iron(III) complexes, the waves Ic and IIc were overlapped (Ic + IIc). Moreover, in the case of some metal complexes, cathodic wave IVc and anodic waves IIIa and IVa could not be detected clearly under the studied experimental conditions.

The cyclic voltammogram of copper(II) complex (figure 4b) showed a new redox couple (I′c/I′a) located at potentials ranging from −0.48 to −0.53 V. The peak separation (ΔE_p) was also 50 mV, indicating that reversible one-electron transfer occurred in the electrode reaction and the observed reaction voltage of the complex was lower than that of the ligand. The presence of peak II′c at about the same potential of ligand wave (IIc) and III′c was near the cathodic window of the $LiClO_4$/DMF system. On the reverse scan, II′a and III′a at more positive potential regions might be due to the products formed at potentials of peak II′c and III′c. All reduction/oxidation steps might have different origins from those obtained for ligand. If successive scans are made, it could be observed that all the processes increase as the number of scans increases. Furthermore, subsequent scans resulted in a gradual increase of the ligand peak II′a, its shape changing from a shoulder to sharp peak. The above voltammetric data showed that Cu(II) was first reduced to Cu(I) and then decomposed copper metal at the cathodic region. At the anodic peak potentials Cu(0) was oxidized to give back Cu(I) and Cu(II) ions, respectively, indicating that processes took place on the metal center of the complex.

From the results obtained between 10 and 500 mV s^{-1}, a plot of logarithm of peak current significantly correlated with the logarithm of scan rate for all metal complexes with slopes between 0.43 and 0.51 (correlation coefficient between 0.997 and 0.999). These findings showed that the redox processes were predominantly diffusion controlled in the whole scan rate range studied. Furthermore, the linear dependence

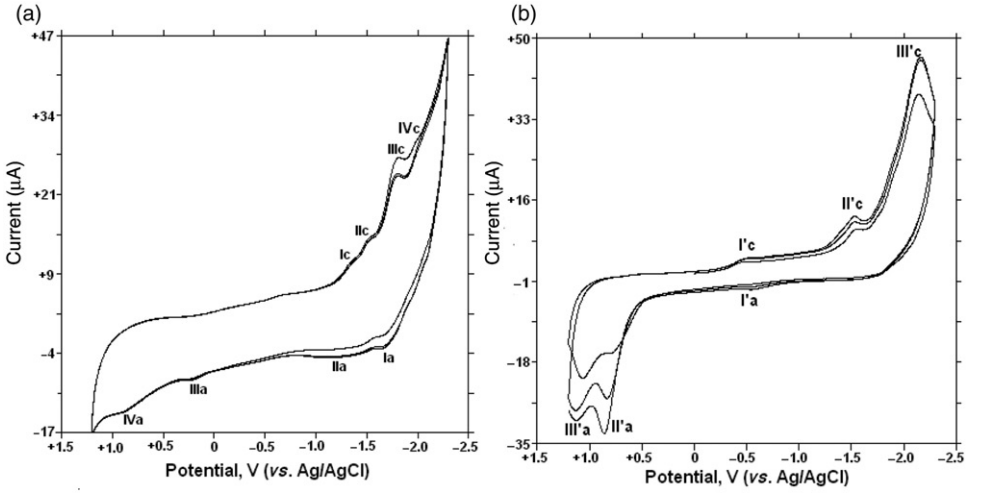

Figure 4. Multisweep cyclic voltammograms of *N*-PMAH (a) and Cu(II) complex (b) solution in DMF at glassy carbon electrode; scan rate, 100 mV s^{-1}.

of the peak current upon the square root of the scan rate with correlation coefficients between 0.991 and 0.999 was found, demonstrating the diffusional behavior.

3.3. *Biological results*

The compounds were screened *in vitro* for their antibacterial activity against four Gram-positive (*S. aureus* ATCC 6538, *S. aureus* ATCC 25923, *B. cereus* ATCC 7064, and *M. luteus* ATCC 9345), one Gram-negative (*E. coli* ATCC 4230) bacteria, and three yeast (*C. albicans* ATCC 14053, *C. krusei* ATCC 6258, and *C. parapsilosis* ATCC 22019) strains by using broth microdilution method. The antibacterial activities of the prepared compounds against Gram-positive and Gram-negative bacteria, expressed as the minimal inhibitory concentrations (MICs), are shown in table 2. As presented in table 3, the ligand and all complexes exhibited weak activity against *E. coli* ATCC 4239 (one Gram-negative bacterium) with MICs in the range of 160–640 $\mu g\,mL^{-1}$. On the contrary, Cu(II), Fe(III), and Ru(III) complexes possessed good antibacterial efficacy

Table 2. MICs[a] of *N*-PMAH and its metal complexes against Gram-negative and Gram-positive bacterial strains.

Compound	*B. cereus* ATCC 7064	*S. aureus* ATCC 6538	*S. aureus* ATCC 25,923	*E. coli* ATCC 4230	*M. luteus* ATCC 9345
N-PMAH	640 ± 00	320 ± 00	320 ± 00	640 ± 00	640 ± 00
$[Cu(N\text{-}PMA)_2]\cdot 2H_2O$	20 ± 00	40 ± 00	40 ± 00	640 ± 00	40 ± 00
$[Co(N\text{-}PMA)_2]\cdot 2H_2O$	640 ± 00	320 ± 00	320 ± 00	640 ± 00	160 ± 00
$[Ni(N\text{-}PMA)_2]\cdot 4H_2O$	640 ± 00	320 ± 00	320 ± 00	640 ± 00	640 ± 00
$[Mn(N\text{-}PMA)_2]\cdot 3H_2O$	320 ± 00	160 ± 00	160 ± 00	320 ± 00	80 ± 00
$[Zn(N\text{-}PMA)_2]\cdot 4H_2O$	640 ± 00	640 ± 00	640 ± 00	640 ± 00	640 ± 00
$[Cd(N\text{-}PMA)_2]\cdot 3H_2O$	80 ± 00	80 ± 00	80 ± 00	320 ± 00	160 ± 00
$[Fe(N\text{-}PMA)_2]Cl\cdot 2H_2O$	40 ± 00	20 ± 00	40 ± 00	160 ± 00	20 ± 00
$[Cr(N\text{-}PMA)_2]Cl\cdot H_2O$	320 ± 00	160 ± 00	160 ± 00	640 ± 00	320 ± 00
$[Ru(N\text{-}PMA)_2]Cl\cdot 3H_2O$	20 ± 00	20 ± 00	20 ± 00	160 ± 00	40 ± 00
Ampicillin	5 ± 00	5 ± 00	10 ± 00	20 ± 00	10 ± 00

[a]The MICs values were determined as $\mu g\,mL^{-1}$ active compounds in medium.

Table 3. MICs[a] of *N*-PMAH and its metal complexes against fungal strains.

Compound	*C. albicans* ATCC 14,053	*C. parapsilosis* ATCC 22,019	*C. krusei* ATCC 6258
N-PMAH	320 ± 00	640 ± 00	320 ± 00
$[Cu(N\text{-}PMA)_2]\cdot 2H_2O$	80 ± 00	80 ± 00	160 ± 00
$[Co(N\text{-}PMA)_2]\cdot 2H_2O$	640 ± 00	640 ± 00	640 ± 00
$[Ni(N\text{-}PMA)_2]\cdot 4H_2O$	–	–	–
$[Mn(N\text{-}PMA)_2]\cdot 3H_2O$	640 ± 00	640 ± 00	1280 ± 00
$[Zn(N\text{-}PMA)_2]\cdot 4H_2O$	640 ± 00	640 ± 00	640 ± 00
$[Cd(N\text{-}PMA)_2]\cdot 3H_2O$	160 ± 00	160 ± 00	80 ± 00
$[Fe(N\text{-}PMA)_2]Cl\cdot 2H_2O$	–	–	–
$[Cr(N\text{-}PMA)_2]Cl\cdot H_2O$	640 ± 00	640 ± 00	640 ± 00
$[Ru(N\text{-}PMA)_2]Cl\cdot 3H_2O$	640 ± 00	640 ± 00	640 ± 00
Fluconazole	5 ± 00	5 ± 00	10 ± 00

[a]Refer footnote of table 2.

against all tested Gram-positive bacteria with MICs between 20 and 80 $\mu g\,mL^{-1}$. Our results also showed that the Ru(III) complex was the most effective compound toward Gram-positive bacterial strains (MIC values 20–40 $\mu g\,mL^{-1}$). However, they had similar or much less active against the tested organisms compared with the standard drug. Additionally, the Cd(II) complex had moderate activity against *B. cereus* ATCC 7064 (one spore-forming Gram-positive bacterium), *S. aureus* ATCC 6538 and *S. aureus* ATCC 25923 (MIC value 80 $\mu g\,mL^{-1}$). Generally, the antibacterial MIC values showed that the efficacy against Gram-positive bacteria was higher than against Gram-negative bacteria.

Table 3 summarizes the antifungal activities of the ligand and its complexes against three yeast strains (*C. albicans* ATCC 14053, *C. krusei* ATCC 6258 and *C. parapsilosis* ATCC 22019). Unfortunately, the ligand and the metal complexes showed poor activity compared with the reference drug. However, the Cu(II) complex exhibited moderate antifungal activity against *C. albicans* ATCC 14053, *C. krusei* ATCC 6258 (MIC, 80 $\mu g\,mL^{-1}$). Although some Ru(II) complexes with the Schiff base salicylamide possessed good antifungal activity [37], our findings demonstrated that Ru(III) containing pyrimidine ring had poor efficacy to the tested fungal strains.

A number of studies reported that the various metal complexes had higher activity against microorganisms than the free ligands, as anticipated from Overtone's concept and chelation theory [37–43]. The data gathered in this study were in good agreement with the previous studies. Indeed, our results revealed that Cu(II), Fe(III), and Ru(III) complexes displayed effective and selective antibacterial activity against the tested Gram-positive bacteria, comparing to the Gram-negative bacteria and *Candida* strains. In this case, low efficacy against the Gram-negative bacteria could be due to the presence of an extra outer membrane in their cell wall acting as barrier foreign substances, such as antibiotics and other antibacterial agents [43]. Fungi had also very rigid and complex formation, including chitin, 80–90% polysaccharide, with proteins, lipids, polyphosphate, and inorganic ions making up the wall-cementing matrix [44]. Here, we propose that the reason for poor anti-yeast activity might be related to the complex and rigid structure of cell wall of fungi.

4. Conclusion

A new heterocyclic ligand containing pyrimidine and Ni(II), Cu(II), Co(II), Mn(II), Zn(II), Cd(II), Cr(III), Fe(III), and Ru(III) complexes were synthesized and characterized. Analytical data, electronic spectra, magnetic susceptibility, IR, and ^{1}H-NMR revealed octahedral geometry for all the complexes. The low conductance values showed non-electrolytic behavior of the complexes, except Fe(III), Cr(III), and Ru(III). Single crystals of the compounds could not be isolated; however, spectroscopic and magnetic data enabled us to predict possible structures. Electrochemical properties of all the compounds were investigated by CV. *N*-PMAH and its complexes were evaluated *in vitro* for the antibacterial and the antimycotic activities against bacteria and yeast. The results obtained from the study indicated that three metal complexes [(Cu(II), Fe(III), and Ru(III)] had effective and selective antibacterial activity against tested Gram-positive bacteria compared to Gram-negative bacteria and *Candida* strains. We speculate two reasons of this higher activity. First, the metal complexes

could be inactivated to several structural enzymes, catalyzing biosynthetic reactions in essential metabolic pathways of the microorganisms. Second, they act as a whole, being able to cross the cell membranes and interfere with the vital cell mechanisms such as DNA replication, transcription, and protein synthesis. Multidrug-resistant microorganisms pose a serious challenge to the medical community and there is urgent need to develop new agents. Some of the new complexes containing pyrimidine could be new antibacterial agents against Gram-positive bacteria.

Acknowledgments

We are grateful to Scientific and Research Council of Turkey (TBAG 105T145) for the support of this research.

References

[1] F. Hueso, N.A. Illan, M.N. Moreno, J.M. Martinez, M.J. Ramirez. *J. Inorg. Biochem.*, **94**, 326 (2003).
[2] M. Sönmez, M. Çelebi, A. Levent, İ. Berber, Z. Şentürk. *J. Coord. Chem.*, **63**, 848 (2010).
[3] S. Roy, T.N. Mandal, A.K. Barik, S. Pal, S. Gupta, A. Hazra, R.J. Butcher, A.D. Hunter, M. Zeller, S.K. Kar. *Polyhedron*, **26**, 2603 (2007).
[4] M. Sönmez, A. Levent, M. Şekerci. *Russian J. Coord. Chem.*, **30**, 695 (2004).
[5] M.A. Girasolo, C. Di Salvo, D. Schillaci, G. Barone, A. Silvestri, G.J. Ruisi. *J. Organomet. Chem.*, **690**, 4773 (2005).
[6] N. Agarwal, P. Srivastava, S.K. Raghuwanshi, D.N. Upadhyay, S. Sinha, P.K. Shulka, V.J. Ram. *Bioorg. Med. Chem.*, **10**, 869 (2002).
[7] B.G. Tweedy. *Phytopathology*, **55**, 910 (1964).
[8] A. Colorado, J. Brodbelt. *J. Mass Spectrom.*, **31**, 403 (1996).
[9] N. Raman, A. Kulandaisamy, C. Thangaraja, P. Manisankar, S. Viswanathan, C. Vedhi. *Transition Met. Chem.*, **29**, 129 (2004).
[10] P.G. Baraldi, M.G. Pavani, N. Nunes, P. Brigidi, B. Vitali, R. Gambari, R. Romagnoli. *Arch. Pharm.*, **10**, 449 (2002).
[11] S.M. Sondhi, M. Johar, S. Rajvanshi, S.G. Dastidar, R. Shukla, R. Raghubir, J.W. Lown. *Aust. J. Chem.*, **54**, 69 (2001).
[12] M.N. Nasr, M.M. Gineinah. *Arch. Pharm.*, **335**, 289 (2002).
[13] N. Kumar, G. Singh, A.K. Yadav. *Heteroat. Chem.*, **12**, 52 (2001).
[14] G. Mangalagiu, M. Ungureanu, G. Grosu, L. Mangalagiu, M. Petrovanu. *Ann. Pharm. Fr.*, **59**, 139 (2001).
[15] Y. Akçamur, B. Altural, E. Sarıpınar, G. Kollenz, O. Kappe, K. Peters, E. Peters, H. Schering. *J. Heterocyl. Chem.*, **25**, 1419 (1988).
[16] National Committee for Clinical Laboratory Standards. *Methods for dilution antimicrobial susceptibility tests for bacteria that grow aerobically, Approved Standard M7-A4*. NCCLS, Villanova, PA, USA (1997).
[17] B.A. Arthington-Skaggs, W. Lee-Yang, M.A. Cıblak, J.P. Frade, M.E. Brandt, R.A. Hajjeh, L.H. Harrison, A.N. Sofair, D.W. Warnock. *Antimicrob. Agents Chemother.*, **46**, 2477 (2002).
[18] M.A. Pfaller, S.A. Messer, S. Coffmann. *J. Clin. Microbiol.*, **33**, 1094 (1995).
[19] National Committee for Clinical Laboratory Standards. *Reference method for broth dilution antifungal susceptibility testing of yeasts, Approved Standard M27-A2*. NCCLS: Wayne, PA, USA (2002).
[20] M. Jadrijevıc-Mladar Takac, D.V. Topic. *Acta Phar.*, **54**, 177 (2004).
[21] K. Nakamoto. *Infrared and Raman Spectra of Inorganic and Coordination Compounds*, Wiley, New York (1986).
[22] M. Sönmez. *Turk. J. Chem.*, **25**, 181 (2001).
[23] S. Deshpande, R. Sharma, T. Srivastava. *Inorg. Chim. Acta*, **78**, 13 (1983).
[24] M. Sönmez, R. Bayram, M. Çelebi. *J. Coord. Chem.*, **62**, 2728 (2009).
[25] M.C. Rakowski, M. Rycheck, D.H. Busch. *Inorg. Chem.*, **14**, 1194 (1975).
[26] A.B.P. Lever. *Inorganic Electronic Spectroscopy*, Elsevier, Amsterdam (1984).
[27] K. Ramareddy, V. Reddy. *Turk. J. Chem.*, **26**, 573 (2002).

[28] M. Sönmez, M. Şekerci. *Polish J. Chem*., **76**, 907 (2002).
[29] K.B. Gudasi, S.A. Patil, R.S. Vadavi, R.V. Shenoy, M.S. Patil. *J. Serb. Chem. Soc*., **71**, 529 (2006).
[30] F.A. Cotton, G. Wilkinson. *Advanced Inorganic Chemistry*, 5th Edn, Wiley-Interscience, New York (1988).
[31] V.K. Sharma, O.P. Pandey, S.K. Sengupta. *J. Inorg. Biochem*., **34**, 253 (1988).
[32] C.J. Ballhausen. *Ligand Field Theory*, McGraw-Hill, New York (1962).
[33] M.M.T. Khan, D. Srinivas, R.I. Kureshy, N.H. Khan. *Inorg. Chem*., **29**, 2320 (1990).
[34] T.D. Thangadurai, S.K. Ihm. *Transition Met. Chem*., **29**, 189 (2004).
[35] E. Laviron. *J. Electroanal. Chem*., **112**, 11 (1980).
[36] H. Kılıç, M. Berkem. *J. Serb. Chem. Soc*., **69**, 689 (2004).
[37] K.V. Sharma, V. Sharma, U.N. Tripathi. *J. Coord. Chem*., **62**, 506 (2009).
[38] S. Kumar, D.N. Dhar, P.N. Saxena. *J. Sci. Ind. Res*., **68**, 181 (2009).
[39] H. Arslan, N. Duran, G. Borekci, C.K. Ozer, C. Akbay. *Molecules*, **14**, 519 (2009).
[40] A. Abdou, M. Mahmoud, Z. Yasser. *Phosphorus, Sulfur Silicon Relat. Elem*., **183**, 1746 (2008).
[41] X.Y. Xu, J. Gao, M.Y. Wang, W.X. Ma, H.B. Song, K.P. Wainwright. *J. Coord. Chem*., **58**, 669 (2005).
[42] A.A. Massoud, V. Langer, L. Öhrstrom, M.A.M. Abu-Youssef. *J. Coord. Chem*., **62**, 519 (2009).
[43] M.T. Madigan, J.M. Martinko, J. Parker. *Brock Biology of Microorganisms*, 8th Edn, Prentice-Hall, Upper Saddle River, NJ, USA (1997).
[44] R. Ramesh, M. Sivagamsundrai. *Synth. React. Inorg. Met.-Org. Chem*., **33**, 899 (2003).